Supporting Information

Mistry et al. 10.1073/pnas.1422576112

SI Materials and Methods

CADD in Silico Screening. In silico screening using CADD followed a previously described protocol (1) adjusted for the present target, the TLR2 TIR domain. The 3D structure of the hTLR2 TIR domain was retrieved from the Protein Data Bank (ID code 1FYW). Charges and hydrogens were added using SYBYL6.4 (Tripos, Inc.). All docking calculations were carried out with the DOCK algorithm (UCSF Computer Graphics Laboratory) (2) using flexible ligands based on the anchored search method (3). The solvent-accessible surface (4) was calculated with the program DMS (UCSF Computer Graphics Laboratory) (5) using a surface density of 2.76 surface points per square angstrom and a probe radius of 1.4 $Å^2$. Sphere sets were calculated with the DOCK-associated program SPHGEN (UCSF Computer Graphics Laboratory). From the full sphere set, sphere clusters in the TLR2 TIR putative "pocket" were identified, where the pocket is adjacent to the BB loop with the conserved proline-guanine (PG) pair and is composed of residues Y641, C673, D678, F679, I680, K683, D687, N688, D691, and S692. The selected sphere set acted as the basis for initial ligand placement during database searching. The GRID method (6) within DOCK was used to approximate the ligand–receptor interaction energy during ligand placement by the sum of the electrostatic and van der Waals (vdW) components. The GRID box dimensions were $41.2 \times 41.7 \times 41.6$ $Å^3$ centered around the sphere set to ensure that docked molecules were within the grid.

A database of more than 1 million low-molecular-weight, commercially available, and FDA-approved compounds was used for the initial virtual screening. This database was created by converting files obtained from the vendors in the 2D spatial data file (SDF) format to the 3D MOL2 format through a procedure that included geometry generation, addition of hydrogens and charges, and force field optimization using SYBYL6.4 along with in-house programs (7, 8). The compounds screened in this manner had between 10 and 40 heavy atoms and less than 10 rotatable bonds. During the docking procedure, each compound was divided into nonoverlapping rigid segments connected by rotatable bonds. Segments with more than five heavy atoms were used as anchors, each of which was docked into the binding site in 250 orientations and minimized. The remainder of the molecule was built around the anchor in a stepwise fashion by adding other segments connected through rotatable bonds. At each step, the dihedral of the rotatable bond was sampled in increments of 10° and the lowest energy conformation was selected. During primary docking, each rotatable bond was minimized as it was created without reminimizing the other bonds. Pruning of the conformational orientations ensured conformational diversity and more favorable energies (9, 10). Energy scoring was performed with a distant-dependent dielectric, with a dielectric constant of 4, and using an all-atom model. Once the whole molecule was built, it was then minimized. The conformation of each molecule with the most favorable interaction energy was selected and saved.

After the primary docking, compounds were chosen for the secondary screening based on their normalized vdW attractive interaction energy scores. Compound selection based on the DOCK energy score favors compounds with a higher molecular weight (MW) because MW contributes to the energy score. To minimize this size bias, an efficient procedure by which the DOCK energies are normalized by the number of heavy atoms N or by a power of N was applied (8): $IE_{norm,vdW} = IE_{vdW}/N^x$. Normalization of the vdW attractive energies was done with x = 1, 0.33, 0.5, and 0.67, and the MW distributions of the top 50,000 compounds in each category were analyzed, with x = 0.33 normalization used for the selection of compounds for secondary screening.

The top 50,000 compounds were subjected to a more rigorous and computationally expensive docking procedure, referred to as secondary database screening. The procedure described for primary docking was followed, with the additional step of minimizing all rotatable bonds simultaneously during the stepwise building of the molecule. In addition, the docking was performed against the crystal conformation and three additional conformations of TLR2 obtained from a molecular dynamics (MD) simulation of the protein. The MD simulation was performed with the program Chemistry at HARvard Macromolecular Mechanics (CHARMM) (11) using the CHARMM22/cross term map (CMAP) force field (12–14) with the TIP3P water model (15) using periodic boundary conditions. The periodic system was a truncated octahedral with a dimension of 86.2 Å, with the protein centered in the simulation box. Two sodium ions were included to yield a neutral system. Electrostatic interactions were treated using particle mesh. The Ewald and Lennard–Jones interactions were truncated over 8–10 Å using force switching (16); nonbond interaction lists were updated heuristically out to 12 Å. Following overlay of the TLR2 protein with water, the system was subjected to a 500-step steepest descent minimization, following which the 5-ns production MD simulation was performed at 298 K using the leap frog integrator with a time step of 2 fs, and SHAKE to constrain all covalent bonds involving hydrogen atoms (17). Coordinates were saved every 1 ns for analysis. Final conformations for docking were selected by rmsd clustering with NMRCLUST (18) on structures from 2 to 5 ns of the MD simulations, with representative structures from the three largest clusters selected for secondary docking. For each compound, the most favorable total interaction energies from the four protein conformations were used for final ranking, from which the top 1,000 compounds were selected and subjected to chemical diversity analysis. Of these 1,000 compounds, we selected the 149 compounds based on chemical diversity and physicochemical properties appropriate for bioavailability (19) and 20 FDA-approved drugs for the ability to block TLR2 signaling.

Reagents. Protein-free LPS from *E. coli* K235 (<0.008% protein) was prepared as a modification of the method used by McIntire et al. (20). P3C and P2C were purchased from EMC Microcollections GmbH. Recombinant mouse and human TNF-α was purchased from eBioscience. *F. tularensis* live vaccine strain (LVS) and *S. pneumoniae* were grown as previously described (21, 22). Heat-killed *S. pneumoniae*, heat-killed *P. aeruginosa*, HKSA, LTA SA, zymosan, poly(I:C), R848, and CpG ODN 1668 were purchased from Invivogen. A QuikChange Lightning Site-Directed Mutagenesis Kit was purchased from Agilent Technologies. *E. coli* was purchased from Life Technologies and heat-killed by heating at 60 °C for 60 min. The C29 (3-[[2-hydroxy-3-methoxyphenyl) methylene] amino]-2-methylbenzoic acid) was purchased from ChemDiv. The *o*-vanillin and 3-amino-2-methylbenzoic acid were purchased from Oakwood. Additional compounds were purchased from Chembridge, Ambinter, and Ryan Scientific. Abs directed against phospho-ERK 1/2, phospho-p38, phospho-JNK 1/2, phospho-p65, IκBα, β-actin, MyD88, and Pan-Cadherin were purchased from Cell Signaling Technology. Anti-hTLR2 Ab was obtained from Abcam.

Cell Culture. Peritoneal exudate macrophages were obtained by peritoneal lavage from 6- to 8-wk-old C57BL/6J mice (The Jackson Laboratory) 4 d after i.p. injection with sterile thioglycollate (Remel) as described (23). Macrophages were washed and cultured in RPMI 1640 supplemented with 2% (vol/vol) FBS, 2 mM glutamine, and 1% penicillin and streptomycin as described (23). Macrophages were plated in six-well tissue culture dishes (4×10^6 cells per well) or in 12-well tissue culture dishes (2×10^6 cells per well). After overnight incubation to allow for adherence of macrophages, cells were treated with the indicated stimuli.

Nontransfected HEK293T cells were maintained in DMEM supplemented with 10% (vol/vol) FBS, 2 mM glutamine, and 1% penicillin and streptomycin. HEK293T cells stably transfected to express hTLR2-YFP (HEK-TLR2), kindly provided by Douglas Golenbock, University of Massachusetts Medical School, Worcester, MA, were enriched in DMEM supplemented with 10% (vol/vol) FBS, 2 mM glutamine, 10 μg/mL ciprofloxacin, and 5 mg/mL G418 Geneticin. THP-1 cells (American Type Culture Collection) were cultured in RPMI 1640 medium modified to contain 2 mM L-glutamine, 10 mM Hepes, 1 mM sodium pyruvate, 4,500 mg/L glucose, and 1,500 mg/L sodium bicarbonate, and were supplemented with 10% (vol/vol) heat-inactivated FBS. THP-1 cells were plated at 2×10^6 cells per well in 12-well tissue culture plates. Cells were cultured with 20 ng/mL phorbol 12-myristate 13-acetate (PMA) for 24 h. Adherent cells were washed twice with THP-1 medium and then treated.

Recombinant Plasmids and Site-Directed Mutagenesis. pcDNA3-YFP-hTLR2 was described previously (24). The NF-κβ–responsive reporter plasmid, pELAM-Luc, was kindly provided by Douglas Golenbock. The pRL-TK-*Renilla* luciferase was obtained from Promega, and pcDNA3.1 was purchased from Invitrogen. The pcDNA3-CFP-hTLR6 and pFLAG-CMV1-hTLR1 were gifts from Andrei Medvedev, University of Connecticut Health Center, Farmington, CT. The pcDNA3.1-mTLR2-CFP, pcDNA3.1-mTLR1-YFP, and pcDNA3.1-mTLR6-CFP plasmids were provided by Vladimir Toshchakov, UMB, Baltimore.

The TLR2 BB loop pocket mutations were introduced into the pcDNA3-YFP-hTLR2 vector using a QuikChange Lightning Site-Directed Mutagenesis Kit (Agilent Technologies) according to the manufacturer's instructions, and the mutation was verified by sequencing.

Preparation of Cell Membrane Fractions. HEK293T cells were transiently transfected with pcDNA3.1, WT pcDNA3-YFP-hTLR2, or mutant TLR2 constructs in the same vector. Forty-eight hours posttransfection, cells were resuspended in homogenization buffer and lysed, and membrane fractions were prepared as described previously (25).

Coimmunoprecipitation and Immunoblotting. Cells were treated and washed once with 1× PBS and lysed using buffer containing 20 mM Hepes (pH 7.4), 150 mM NaCl, 1 mM EDTA, 1 mM EGTA (pH 8.0), 50 mM NaF, 0.5% Triton X-100, 1 mM Na_3VO_4, 1 mM DTT, 1 mM PMSF, and protease inhibitor (Roche Applied Science). Cells were harvested, and protein was quantified using BCA Protein Assay Reagents (Thermo Scientific/Pierce). Whole-cell lysates (500 μg per 500 μL) were precleared using 10 μL of prewashed Protein G Agarose (Roche Applied Science) for 2 h at 4 °C with rotation. Precleared samples were incubated with the respective Ab and rotated overnight at 4 °C. Prewashed protein G (40 μL) was added to each sample and rotated for 4 h at 4 °C. Beads were washed three times in lysis buffer (without protease inhibitor) and finally in complete lysis buffer. Beads were resuspended in 2× Laemmli sample buffer and boiled for 10 min. Immunoprecipitated proteins were separated by 10% SDS/PAGE, transferred onto a PVDF membrane, blocked, and incubated with the respective primary and secondary Abs, and bands were visualized using ECL Plus Reagents (Amersham Pharmacia Biotech) as described (26).

Evaluation of Cellular Cytotoxicity. Cellular cytotoxicity was determined by measuring lactate dehydrogenase activity released in the media after treatment with TLR agonist or TNF-α in the presence of media, vehicle (NaOH), or C29 using the CytoTox 96 Non-Radioactive Cytotoxicity Assay (Promega) and quantified by measuring wavelength A at 490 nm. Treatment of cells with Triton X-100 served as the positive control.

1. Hancock CN, et al. (2005) Identification of novel extracellular signal-regulated kinase docking domain inhibitors. *J Med Chem* 48(14):4586–4595.
2. Kuntz ID, Blaney JM, Oatley SJ, Langridge R, Ferrin TE (1982) A geometric approach to macromolecule-ligand interactions. *J Mol Biol* 161(2):269–288.
3. Kuntz ID (1992) Structure-based strategies for drug design and discovery. *Science* 257(5073):1078–1082.
4. Connolly ML (1983) Solvent-accessible surfaces of proteins and nucleic acids. *Science* 221(4612):709–713.
5. Ferrin TE, et al. (1988) The MIDAS display system. *J Mol Graph* 6(1):13–27.
6. Goodford PJ (1984) Drug design by the method of receptor fit. *J Med Chem* 27(5):558–564.
7. Huang N, Nagarsekar A, Xia G, Hayashi J, MacKerell AD, Jr (2004) Identification of non-phosphate-containing small molecular weight inhibitors of the tyrosine kinase p56 Lck SH2 domain via in silico screening against the pY + 3 binding site. *J Med Chem* 47(14):3502–3511.
8. Pan Y, Huang N, Cho S, MacKerell AD, Jr (2003) Consideration of molecular weight during compound selection in virtual target-based database screening. *J Chem Inf Comput Sci* 43(1):267–272.
9. Ewing TJ, Kuntz ID (1997) Critical evaluation of search algorithms used in automated molecular docking. *J Comput Chem* 18(9):1175–1189.
10. Leach AR, Kuntz ID (1992) Conformational analysis of flexible ligands in macromolecular receptor sites. *J Comput Chem* 13(6):730–748.
11. Brooks BR, et al. (2009) CHARMM: The biomolecular simulation program. *J Comput Chem* 30(10):1545–1614.
12. MacKerell AD, Jr, et al. (1998) CHARMM: The Energy Function and Its Paramerization with an Overview of the Program. *Encyclopedia of Computational Chemistry*, eds Schleyer PvR, et al. (Wiley, Chichester, UK), Vol 1, pp 271–277.
13. MacKerell AD, Jr, Feig M, Brooks CL, III (2004) Improved treatment of the protein backbone in empirical force fields. *J Am Chem Soc* 126(3):698–699.
14. Mackerell AD, Jr, Feig M, Brooks CL, 3rd (2004) Extending the treatment of backbone energetics in protein force fields: Limitations of gas-phase quantum mechanics in reproducing protein conformational distributions in molecular dynamics simulations. *J Comput Chem* 25(11):1400–1415.
15. Jorgensen WL, Chandrasekhar J, Madura JD, Impey RW, Klein ML (1983) Comparison of simple potential functions for simulating liquid water. *J Chem Phys* 79(2):926–935.
16. Steinbach PJ, Brooks BR (1994) New spherical-cutoff methods of long-range forces in macromolecular simulations. *J Comput Chem* 15(7):667–683.
17. Ryckaert JP, Ciccotti G, Berendsen HJC (1977) Numerical integration of the Cartesian equations of motion of a system with constraints: Molecular dynamics of n-alkanes. *J Comput Phys* 23(3):327–341.
18. Kelley LA, Gardner SP, Sutcliffe MJ (1996) An automated approach for clustering an ensemble of NMR-derived protein structures into conformationally related subfamilies. *Protein Eng* 9(11):1063–1065.
19. Lipinski CA (2000) Drug-like properties and the causes of poor solubility and poor permeability. *J Pharmacol Toxicol Methods* 44(1):235–249.
20. McIntire FC, Sievert HW, Barlow GH, Finley RA, Lee AY (1967) Chemical, physical, biological properties of a lipopolysaccharide from Escherichia coli K-235. *Biochemistry* 6(8):2363–2372.
21. Cole LE, et al. (2006) Immunologic consequences of Francisella tularensis live vaccine strain infection: Role of the innate immune response in infection and immunity. *J Immunol* 176(11):6888–6899.
22. Pennini ME, Perkins DJ, Salazar AM, Lipsky M, Vogel SN (2013) Complete dependence on IRAK4 kinase activity in TLR2, but not TLR4, signaling pathways underlies decreased cytokine production and increased susceptibility to Streptococcus pneumoniae infection in IRAK4 kinase-inactive mice. *J Immunol* 190(1):307–316.
23. Salkowski CA, et al. (1999) IL-12 is dysregulated in macrophages from IRF-1 and IRF-2 knockout mice. *J Immunol* 163(3):1529–1536.
24. Xiong Y, Song C, Snyder GA, Sundberg EJ, Medvedev AE (2012) R753Q polymorphism inhibits Toll-like receptor (TLR) 2 tyrosine phosphorylation, dimerization with TLR6, and recruitment of myeloid differentiation primary response protein 88. *J Biol Chem* 287(45):38327–38337.
25. Bhat N, et al. (1999) Use of a photoactivatable taxol analogue to identify unique cellular targets in murine macrophages: Identification of murine CD18 as a major taxol-binding protein and a role for Mac-1 in taxol-induced gene expression. *J Immunol* 162(12):7335–7342.
26. Polumuri SK, et al. (2012) Transcriptional regulation of murine IL-33 by TLR and non-TLR agonists. *J Immunol* 189(1):50–60.

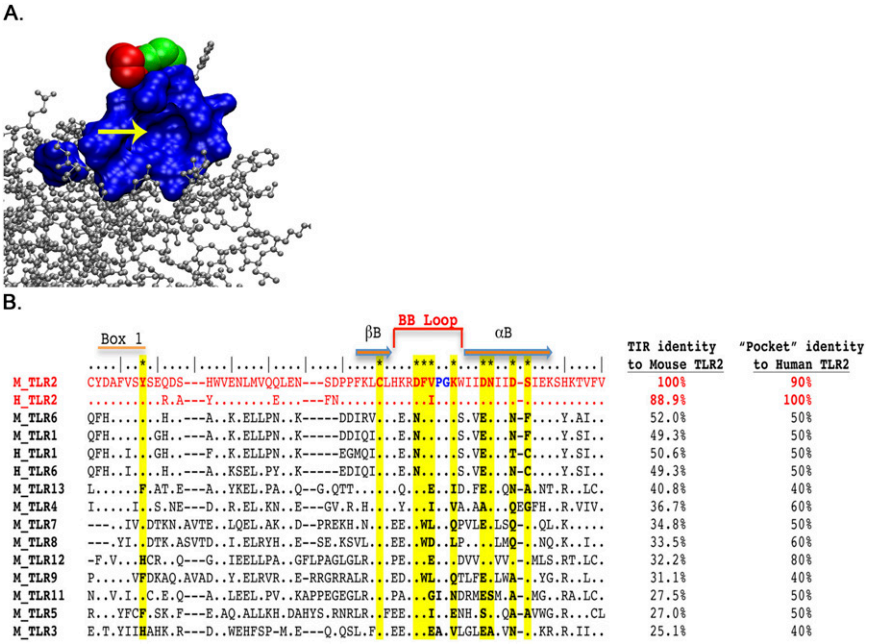

Fig. S1. TLR2 TIR structure and alignment. (*A*) Molecular model of the TLR2 TIR domain (Protein Data Bank ID code 1FYW) (silver) with an arrow indicating the CADD-targeted BB loop pocket (blue). Conserved P681 (red) and G682 (green) residues of the BB loop are found adjacent to the CADD-targeted pocket. The Visual Molecular Dynamics program was used to generate this molecular model (1). (*B*) Comparison of TIR domains from mouse (M) and human (H) TLRs based on amino acid alignment. Residues identical to the mouse TLR2 sequence are indicated with a dot. Yellow highlighting and bold type beneath the asterisks (*) indicate residues that form the CADD-targeted pocket. Bold type in blue identifies the conserved P681–G682 residues of the BB loop. The percentage of protein identity across the entire TIR domain and the CADD-targeted pocket is given.

1. Humphrey W, Dalke A, Schulten K (1996) VMD: Visual molecular dynamics. *J Mol Graph* 14(1):33–38.

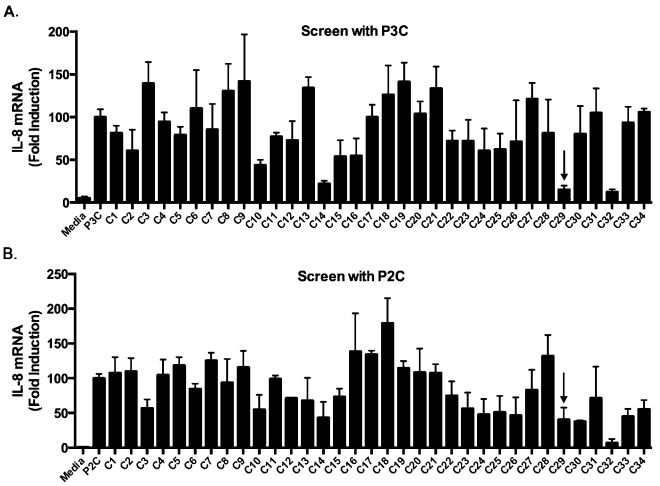

Fig. S2. Initial in vitro screening of potential TLR2 inhibitors. Total RNA was extracted from HEK-TLR2 cells pretreated for 1 h with 100 μM indicated compound and then stimulated with P3C (100 ng/mL; *A*) or P2C (5 ng/mL; *B*) for 1 h in the presence of the compound. IL-8 mRNA was measured as described in Fig. 1*B*. The arrow indicates C29. The qRT results shown are the mean ± SEM from at least three independent experiments, each carried out in duplicate.

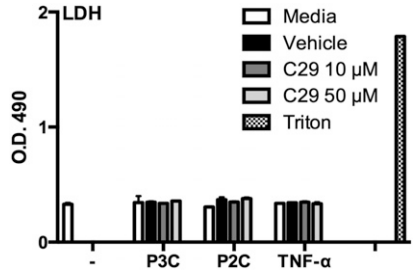

Fig. S3. C29 is not cytotoxic to HEK-TLR2 stable transfectants. Cells were pretreated for 1 h with media, vehicle (65 μM NaOH), or C29 (10 μM or 50 μM) and then stimulated with P3C (200 ng/mL), P2C (200 ng/mL), or human TNF-α (300 ng/mL) for 1 h in the presence of media, vehicle, or C29. Supernatants of cell cultures were collected and analyzed for lactate dehydrogenase (LDH) release as a measure of cell cytotoxicity with Triton X-100–lysed cells serving as the positive control. LDH release is representative of one of two independent experiments carried out in duplicate.

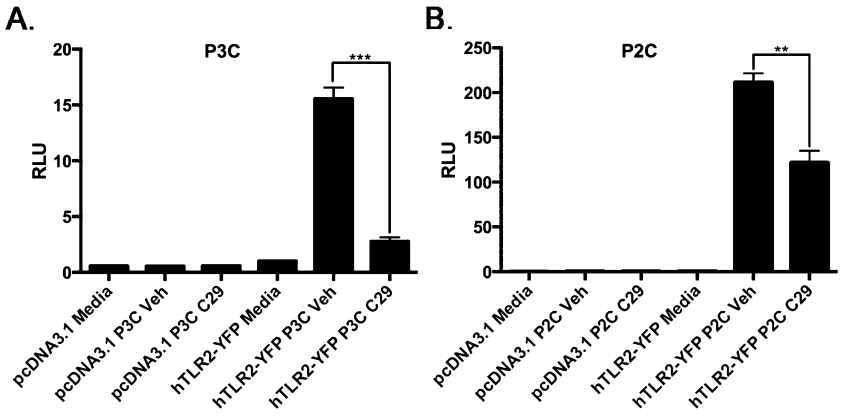

Fig. S4. C29 inhibits hTLR2/1- and hTLR2/6-induced NF-κB activation. (*A* and *B*) HEK293T cells were transiently transfected with reporter constructs for endothelial leukocyte adhesion molecule (ELAM)-luciferase, *Renilla*-luciferase, and either pcDNA3.1 or pcDNA3-YFP-hTLR2. Cells were pretreated for 1 h with media, vehicle (Veh; 65 μM NaOH), or C29 (50 μM) and treated with P3C or P2C (50 ng/mL) for 5 h in the presence of media, vehicle, or C29. Lysates were prepared, and the dual-luciferase assay was performed. Results are representative of three independent experiments, each carried out in duplicate (**$P \leq 0.01$; ***$P \leq 0.001$). RLU, relative luciferase unit.

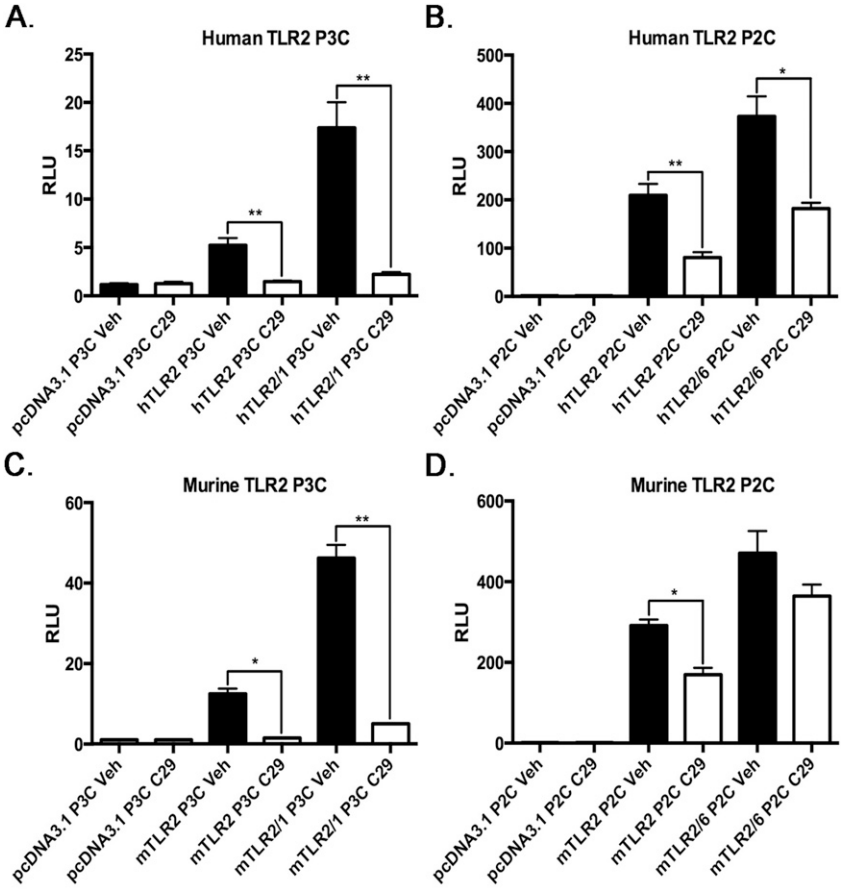

Fig. S5. C29 is species-specific and blocks hTLR2/6 signaling but not mTLR2/6 signaling. (*A–D*) HEK293T cells were transiently transfected with reporter constructs for ELAM-luciferase, *Renilla*-luciferase, and pcDNA3.1 in combination with/without pcDNA3-YFP-hTLR2, pFLAG-CMV1-hTLR1, pcDNA3-CFP-hTLR6, pcDNA3.1-mTLR2-CFP, pcDNA3.1-mTLR1-YFP, or pcDNA3.1-mTLR6-CFP. Cells were pretreated for 1 h with media, vehicle (65 μM NaOH), or C29 (50 μM) and then treated with P3C or P2C (50 ng/mL) for 5 h in the presence of media, vehicle, or C29. Lysates were prepared, and the dual-luciferase assay was performed. *A* and *B* represent the mean ± SEM from three independent experiments, and *C* and *D* represent the mean ± SEM from two independent experiments, each carried out in duplicate (**P* ≤ 0.05; ***P* ≤ 0.01).

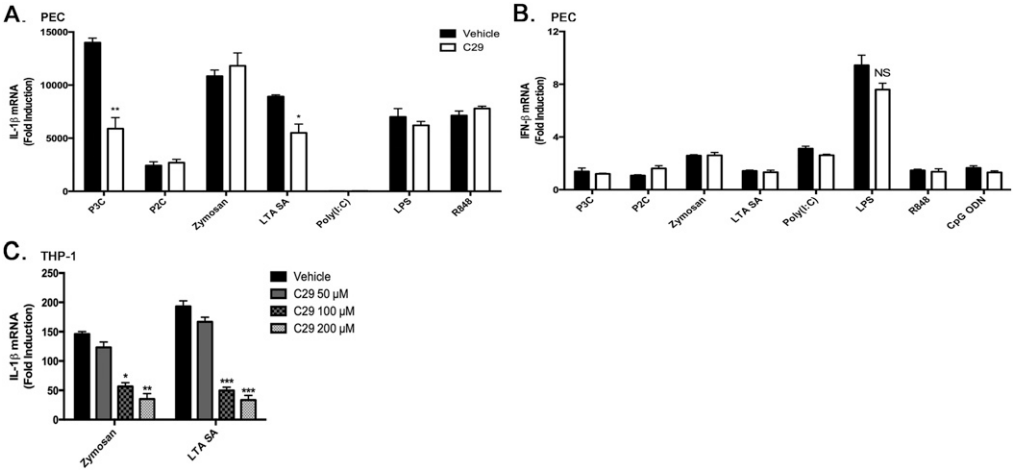

Fig. S6. Examining the broader specificity of C29 for TLR2 signaling. (*A* and *B*) Total RNA was extracted from murine macrophages that had been pretreated for 1 h with vehicle (65 μM NaOH) or C29 (50 μM) and then stimulated with P3C (50 ng/mL), P2C (100 ng/mL), zymosan (10 μg/mL), LTA SA (1 μg/mL), poly(I:C) (10 μg/mL), LPS (100 ng/mL), R848 (10 μg/mL), or CpG ODN 1668 (5 μM) for 3 h in the presence of vehicle or C29. IL-1β and IFN-β mRNA were measured as described in Fig. 1*D*. (*C*) THP-1 cells were plated in the presence of phorbol 12-myristate 13-acetate (PMA; 20 ng/mL) for 24 h and washed twice in media. Total RNA was extracted from cell cultures pretreated for 1 h with vehicle (260 μM NaOH) or C29 (50 μM, 100 μM, or 200 μM) and then stimulated with zymosan (10 μg/mL) or LTA SA (1 μg/mL) for 4 h in the presence of vehicle or C29. IL-1β mRNA was measured as described in Fig. 1*B*. The qRT results represent the mean ± SEM from two independent experiments, each carried out in duplicate (**P* ≤ 0.05; ***P* ≤ 0.01; ****P* ≤ 0.001).

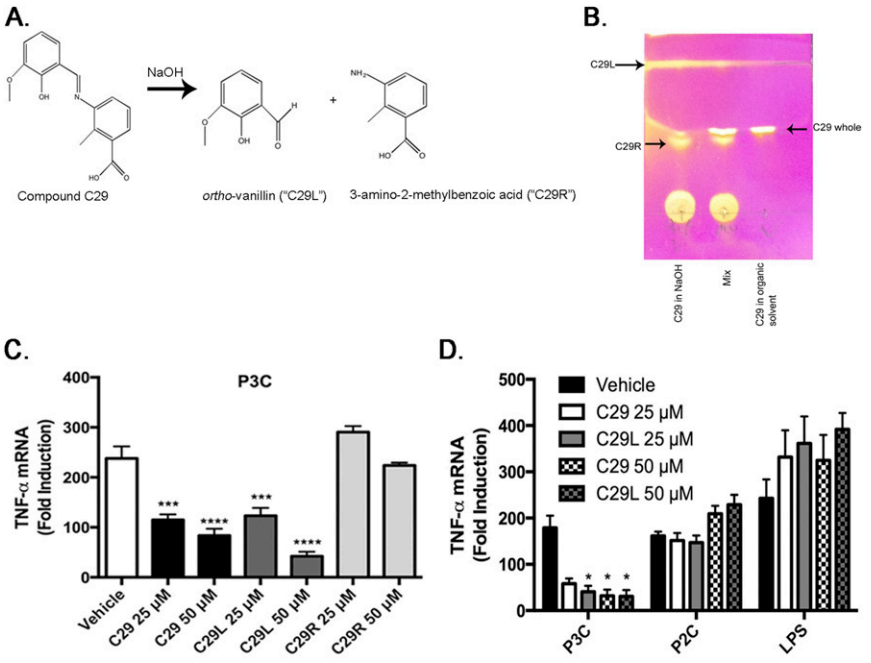

Fig. S7. C29L reproduces the TLR2 inhibitory activity observed with C29. (*A*) C29 dissolved in NaOH generates C29L and C29R. (*B*) TLC plate coated with silica was spotted with C29 dissolved in 65 μM NaOH, C29 dissolved in ethyl acetate (organic solvent), and a mixture of both. The plate was placed in solvent and visualized using a $KMnO_4$ stain. (*C* and *D*) Total RNA was extracted from murine peritoneal macrophages that had been pretreated for 1 h with vehicle (65 μM NaOH), C29 (25 μM or 50 μM), C29L (25 μM or 50 μM), or C29R (25 μM or 50 μM) and then stimulated with P3C (50 ng/mL), P2C (100 ng/mL), or LPS (100 ng/mL) for 1 h in the presence of vehicle, C29, C29L, or C29R. TNF-α mRNA was measured as described in Fig. 1*D*. The qRT results are representative of two independent experiments, each carried out in duplicate (*$P \leq 0.05$; **$P \leq 0.01$; ***$P \leq 0.001$; ****$P \leq 0.0001$).

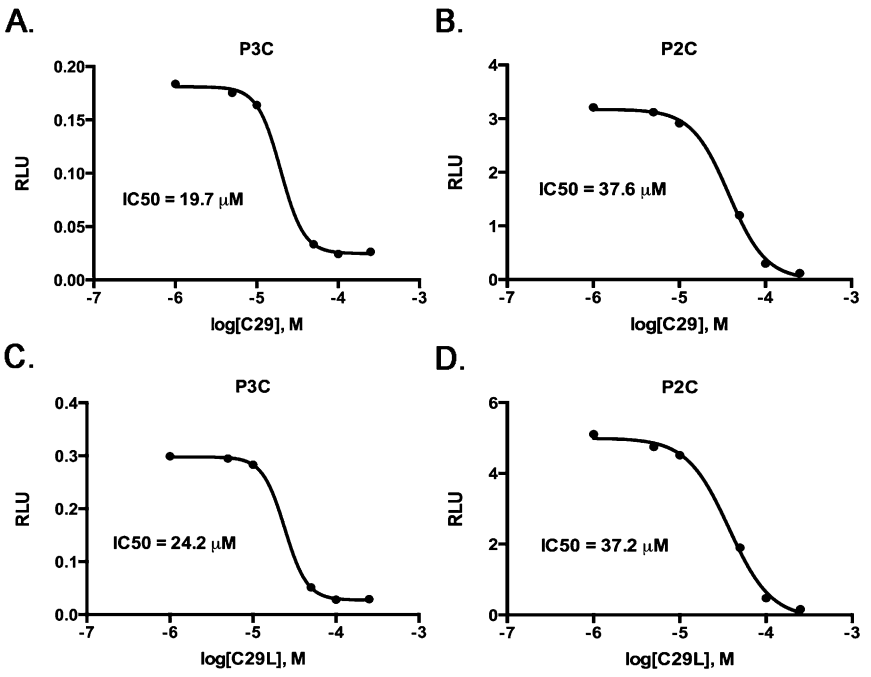

Fig. S8. C29L blocks hTLR2/1 and hTLR2/6 signaling comparable to C29 in HEK293T cells. (*A–D*) HEK293T cells were transiently transfected with reporter constructs for ELAM-luciferase, *Renilla*-luciferase, and pcDNA3-YFP-hTLR2. Cells were pretreated for 1 h with C29 or C29L (1–250 μM) and treated with P3C or P2C (50 ng/mL) for 5 h in the presence of C29 or C29L. Lysates were prepared, and a dual-luciferase assay was performed. Data are representative of two independent experiments, each carried out in duplicate.

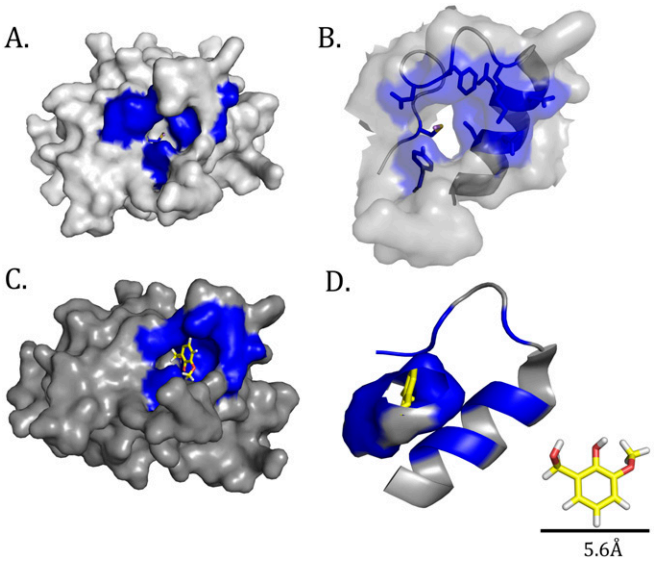

Fig. S9. Surface representation of the BB loop pocket modeled with C29L. (*A*) Surface representation of the BB loop pocket. Residues that comprise the BB loop pocket (Y647, C673, D678, F679, I680, K683, D687, N688, D691, and S692) are highlighted in blue. (*B*) Close-up depiction of the BB loop pocket showing both the surface representation and underlying secondary structure and the BB loop pocket residues (highlighted in blue). (*C* and *D*) Surface representation of the solvent-accessible BB loop pocket with C29L modeled into this pocket [C29L with carbon (yellow), oxygen (red), and hydrogen (gray) atoms is depicted in *D*, *Lower Right*].

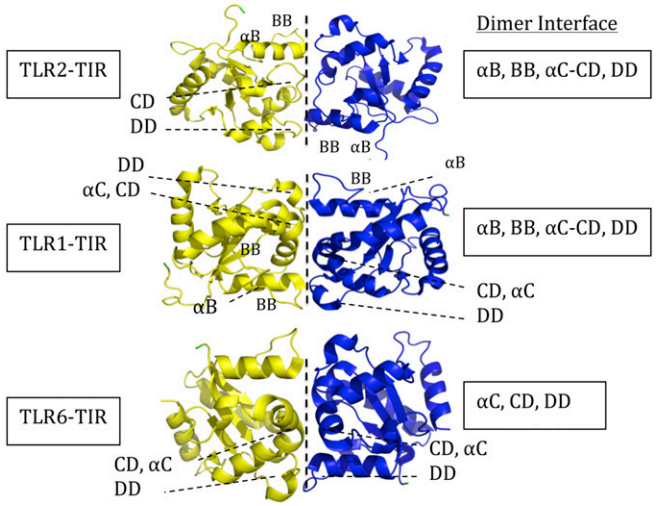

Fig. S10. Cartoon representation of the homodimeric interactions observed in the crystal structures of TIR1 [Protein Data Bank (PDB) ID code 1FYV], TIR2 (PDB ID code 1FYW), and TIR6 (PDB ID code 4OM7) with interacting loops and helices. The dimeric interfaces of TIR1 and TIR2 involve BB, CD, and DD loops along with either α-C or α-B helices to mediate dimerization. In contrast, the interface of the TIR6 dimer primarily uses the CD loop, DD loop, and α-C helix to mediate dimerization and does not involve the BB loop.